JOURNAL OF THERMOPHYSICS AND HEAT TRANSFER
Vol. 25, No. 1, January–March 2011

Backward-Facing Step Flow in Microchannels Using Microparticle Image Velocimetry

Ehsan Yakhshi-Tafti, Hyoung J. Cho, and Ranganathan Kumar*
University of Central Florida, Orlando, Florida 32816

DOI: 10.2514/1.42910

Flow at a backward-facing step feature (1:5 expansion ratio) in a microchannel has been studied using microparticle image velocimetry. The onset and development of a recirculation flow was studied as a function of flow rate. The onset of recirculation was initiated at flow rates that correspond to Reynolds numbers, $Re > 95$. The dimensions are such that recirculation flow has a three-dimensional structure and is expected to vary with the depth coordinate. Because of volume illumination, most microparticle-image-velocimetry measurements provide two-dimensional averaged flow profiles. Flow at the backward-facing step offers the opportunity to investigate the ability of resolving the depth dependency by conventional microparticle image velocimetry in relevance to two parameters: variation of the focus plane depth z^* and using variable time intervals for particle-image-velocimetry image pairs Δt. The ensemble cross-correlation algorithm was found to be insensitive to the variation of z^* for low magnification (4x) but was able to resolve the parabolic nature of flow across the depth of the channel, when high magnification objective lenses were used (20x). For a given flow rate and constant z^*, the variation of Δt resulted in quantitatively and qualitatively different flow patterns, suggesting that Δt is an indirect means of resolving the depth as the correlation algorithm locks onto a flow plane with particles moving at a speed that can be resolved with the given process parameters and time interval.

Nomenclature

A	=	channel cross-sectional area, μm^2
D_H	=	hydraulic diameter, μm; $4A/P$
H	=	channel height, μm
N	=	number of image pairs in particle-image-velocity correlation
P	=	channel perimeter, L/ min
Q	=	flow rate, μL/ min
Re	=	Reynolds number; $\rho U D_H/\mu$
w	=	channel width, μm
z^*	=	normalized focus plane depth; z/H
Δt	=	time interval between particle-image-velocity image pairs
Φ	=	correlation function

I. Introduction

MICROPARTICLE image velocimetry (μPIV) is a useful tool in studying small-scale flow and related phenomena in microfluidics. In comparison with conventional particle image velocimetry (PIV), the μPIV technique requires that the tracer particles be in the size range of the wavelength of the illumination light. The Brownian motion of tracing particles can be a source of error in low rates of flow. The illumination of the flow is not in a two-dimensional (2-D) plane, as in conventional PIV, but in an illumination volume. Hence, out-of-focus emissions from particles below and above the focus plane increase the noise-to-signal ratio. In addition to visualizing the onset and development of recirculation in microchannel flows, the purpose of this study is to investigate the effect of variables affecting μPIV in relevance to volume illumination: variation of the focus plane depth and time intervals between the PIV image pairs in a backward-facing step. An ensemble cross-correlation scheme was used to derive the flowfield.

In conventional PIV, the thickness of the illumination light sheet is much smaller than the characteristic dimensions of the flow, so that the flow can be analyzed layer by layer. In μPIV, however, all the particles in the flowfield are illuminated due to limited optical access; the intensity of light scattered by the tracer particles varies depending on their location from the plane of focus. The epifluorescence technique is implemented in μPIV, since the limited optical access does not allow illumination and collection of the excitation and reemission light from two separate paths. Fluorescent dyes offer the possibility of using only one optical pathway. Excitation light from a neodymium-doped yttrium aluminum garnet (ND:YAG) laser with a fixed wavelength is guided to the desired location of the flow; fluorescent dyes absorb this light, moving into an excitation mode. Upon releasing the absorbed energy, they reemit light at a higher wavelength (part of the energy gets dissipated). The reemission light can be filtered out using a dichroic mirror that is transparent to the wavelength used for excitation but reflective to the reemission wavelength. The reemission light is guided to the charge-coupled device (CCD) camera, where the images are recorded in pairs and eventually transmitted to a computer for further processing. The fact that all particles in the field of view are illuminated can be a major problem. The light from particles off the plane of focus forms a background noise (glow) that makes it difficult to distinguish between light scattered from in-focus particles and that from the off-focus particles. In most cases, information regarding the depthwise behavior of the flow is lost, and a 2-D average field is derived [1]. Two approaches are possible:

1) Choose the depth of field to be larger than the thickness of the flow. The depth can further be resolved by filtering techniques based on the intensity of light [2].

2) Choose the depth of focus to be significantly narrower than the depth of flow; in this sense, only a narrow slice of the flow would be in focus, and the light from seeding particles above or below the plane will be considered as noise [3].

Olsen and Adrian [4,5] introduced the concept of particle visibility for μPIV measurements while addressing this issue. Particles were considered to be visible if only their peak intensity in the recorded images rose significantly above the background glow. Particle visibility increases by decreasing the f number of the optical system; the depth of field increases by increasing the f number. This means that images taken with a low f number will tend to have a limited

Presented as Paper 2009-1584 at the 47th AIAA Aerospace Sciences Meeting, Including The New Horizons Forum and Aerospace Exposition, Orlando, FL, 5–8 January 2009; received 23 December 2008; revision received 18 August 2010; accepted for publication 23 August 2010.

*Mechanical Material and Aerospace Engineering, 4000 Central Florida Boulevard; Rnkumar@mail.ucf.edu.

number of particles in focus, with the rest being out of focus, thus eliminating the contribution of out-of-focus particles.

Meinhart et al. [3,6] maintained high spatial resolution at low particle concentration by taking many realizations and then averaging the calculated spatial correlations for each interrogation region to yield a high-vector-density velocity field. This technique is limited to steady flows or periodic flows with phase locking. Usually, the measured velocity is found to be a weighted average over the depth of the fluidic device. By using appropriate weighting functions, the velocity variation from top to bottom of the interrogation volume can be accounted for. The weighting function can be used to put a bound on the interrogation volume (depth of correlation) by defining a distance from the object plane beyond which particles no longer contribute to the correlation function significantly. As a solution for the background noise reduction, Bourdon et al. [7] proposed an image-filtering method, termed power filtering, for controlling the depth of correlation, independent of the image acquisition system, particle size, and flow characteristics. By choosing appropriate power values, it is possible to increase or decrease the depth of correlation by a factor of two.

The recirculation flow at a backward-facing step feature in a microchannel is chosen to evaluate the ability of an ensemble cross-correlation μPIV algorithm using volume illumination in resolving the flow in the depth coordinates. Because of the high width-to-depth ratio (10:1), the vortex generated at the sudden expansion is highly dependent on the depth coordinate. The eye of the vortex, the area affected by the recirculation, and the magnitude of velocities and other characteristics of the flow vary differently from one depth to another. Therefore, the recirculation flow at the backstep lends itself well to the study of depth resolution in μPIV. In addition, this setup provides an opportunity to study transition to recirculation flow in microchannels, which is of relevance to microfluidics applications such as the study of transport phenomena and the design of micromixers and cooling applications.

Flow separation and recirculation are the main flow features at sudden expansion geometries in internal macroscopic flows. Sudden expansion (backward-facing step) flows are among the commonly occurring basic flow patterns. Armaly et al. [8] used laser-Doppler anemometry to make comprehensive measurements on air flows over a backward-facing step in a macrochannel over a 70–8000 range of Reynolds number, covering laminar, transitional, and turbulent flows. Many numerical works have also been reported on this subject. Biswas et al. [9] studied backward-facing step flow for expansion ratios of 1.95, 2, and 3 and provided information on characteristic flow patterns for Re of 10^{-4} to 800. The objective of this paper is to evaluate the possibility of resolving the depthwise behavior of flow using volume illumination and the ensemble cross-correlation μPIV algorithm, considering the effect of the variation of the focus plane depth and the time intervals between PIV image pairs.

II. Experimental Setup

The microfluidic device used for this study is fabricated using the well established SU-8 photolithography and polydimethylsiloxane (PDMS) replication techniques [10]. The device pattern is transferred via photolithography from a mask onto the silicon wafer, which has been spin coated with SU-8 photoresist (PR). The developed SU-8 on the wafer is used as a mold; PDMS with a curing agent is poured on the mold and allowed to cure overnight at room temperature. The PDMS layer with cast features is then bonded to another flat piece of PDMS or glass slide by plasma surface treatment. The device consists of a straight channel with a rectangular cross section that suddenly expands to a larger width (1:5 ratio). The spin-coating speed of SU-8 on the silicon wafer determines the thickness of the film. As mentioned earlier, the patterns transferred to the SU-8 film via photolithography serve as the mold, which is eventually used to cast the patterns onto the PDMS resin to form the microchannels. The device height in this study was in the range of 100 to 120 μm; height variation was due to variables of the fabrication process, such as spin-coating speed and PR viscosity (Fig. 1).

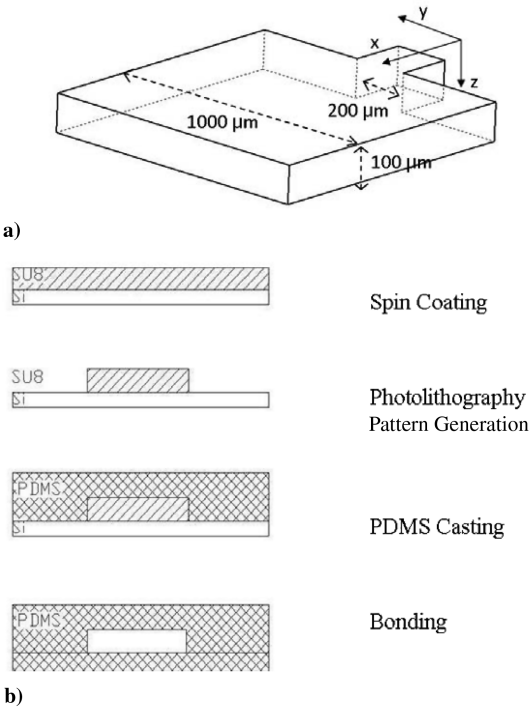

Fig. 1 Microchannel: a) three-dimensional view of the backward-facing step and b) procedure used in the fabrication.

Recirculation flow occurs as the flow suddenly expands at the backward-facing step feature. The channel width-to-height ratio is 10:1 (x: flow direction, z: depth) downstream of the expansion, and the flow is highly dependent on the depth coordinate due to the no-slip boundary condition at the top and bottom walls. The characteristics of the recirculation flow in this setup vary noticeably from near the wall to the center of the channel (the center of the vortex, the area affected by recirculation, and the location of the reattachment streamlines, etc. are depth dependent). This configuration provides a suitable case to study the ability of μPIV algorithms in resolving the depth coordinate of flows where volume illumination is used.

The μPIV (TSI, Inc., Shoreview, Minnesota) setup consisted of an ND:YAG laser (532 nm), a Nikon (TE2000-S) inverted microscope, 4x and 20x magnifying objective lenses, and a barrier filter cube to filter out the reemission light from the excitation light (Fig. 2). Polystyrene fluorescent dye was used as the tracer particle with the following properties: 1 μm average diameter, 540 nm excitation/560 nm reemission wavelength, and 10^{10} beads/mL (FluoroSpheres, Invitrogen, Calfornia). A CCD camera was used to capture PIV images; it was capable of acquiring image pairs at a maximum of 15 double-image frames per second, with time intervals between two images as low as 1 μs. The timings of the laser firing and image capture were controlled by a synchronizer unit. The ensemble cross-correlation scheme together with background conditioning was used for deriving the flowfield from the captured images. The ensemble correlation was appropriate for visualization of steady flow patterns. The correlation function at a certain interrogation spot is generally represented by the following [11]:

$$\Phi_k(m,n) = \sum_{j=1}^{q}\sum_{i=1}^{p} f_k(i,j)\cdot g_k(i+m, j+n) \qquad (1)$$

where f and g are the gray value distribution from the first and second exposure for the kth recording PIV pair on an interrogation spot of size $(p \times q)$ pixels. In the current experiment, the Nyquist grid generation scheme is used, which gives a vector grid with a 50% interrogation spot overlap required by the Nyquist sampling criteria. The interrogation spots are chosen to be 32×32 pixels. The highest peak of this function occurs at the particle-image displacement in the interrogation spot. The fast Fourier transform is used to form the

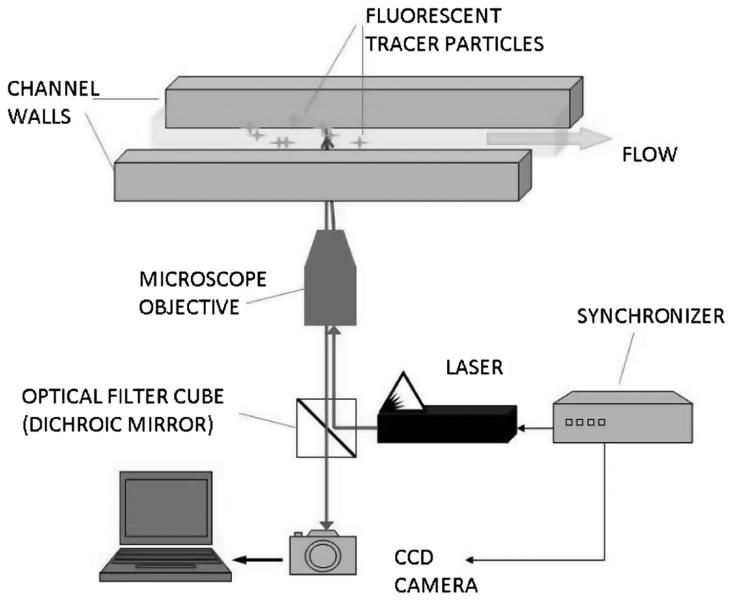

a)

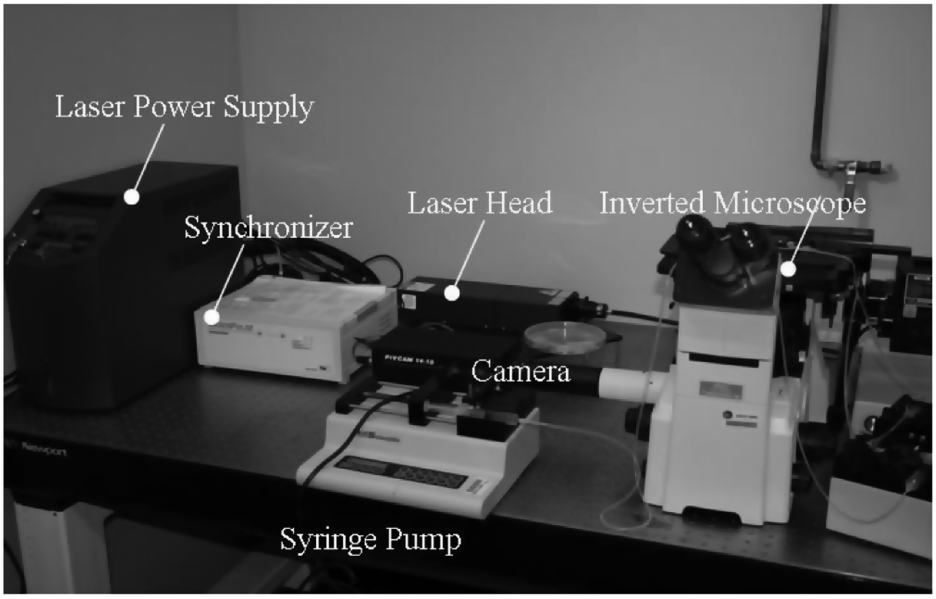

b)

Fig. 2 μPIV a) schematic of the system with the inverted microscope and the associated optics and b) photograph of the experimental setup.

correlation map, and a Gaussian peak finder is used to find the displacement peak within the specified displacement bounds using a three-point fit done in the x and y directions. The highest peak is set as the displacement peak, and the second maximum is set as the noise peak. The ratio of the main displacement peak to the noise peak is set to a threshold value of 1.5; that is, the amplitude of the main displacement peak should be 1.5 larger than the noise peak for it to be considered valid. The random error associated with the determination of the position of the correlation peak is largest when the maximum displacement within the interrogation spots are very small compared with the dimensions of the interrogation spot; this error is limited to under 10% for the displacement of 2 pixels, and more in a 32×32 interrogation window [12]. On the other hand, increasing the maximum displacement allowed within an interrogation spot would cause loss of correlation pairs. In the current experiments, 15 pixels are chosen for the maximum displacement allowed in each correlation pair. Since the flow is steady, the main peak of $\Phi_k(m, n)$ should occur at the same position for all the PIV recordings, whereas other subpeaks would be located at random spots in the imaging domain. The average (ensemble) correlation is given as

$$\Phi_{\text{ens}}(m, n) = 1/N \sum_{k=1}^{N} \Phi_k(m, n) \tag{2}$$

where N is the number of realizations. Random errors in numerical processing inherent to grid generation, correlation, and peak finding algorithms become negligible by increasing the number of realizations. An average of $N = 50$ image pairs were required to yield vector fields with reasonable quality and spatial resolution.

III. Measurement Uncertainty

When the particle image is small compared with the pixel size, the bias error becomes significant because of the finite numerical resolution of the correlation function. If the particle image is large, random error due to irregularities in the images will dominate [13].

Therefore, a tracer particle size should be smallest in the absolute sense for not disturbing the flow, but it should be large compared to pixel size. For example, if the diameter of a particle image is resolved over 3 to 4 pixels, then the uncertainty in determining particle displacement can be found to within one tenth of the particle-image diameter [14]. The camera records digital images of 512×480 pixels of an area of 600×400 μm, resulting in ~ 1 μm^2/pixel. Since seeding particles occupy approximately 3 pixels (projected area of a particle is 3.14 μm^2), the displacement of each particle is found to be 0.1 μm accurate. Using an average of 200 μs time intervals in the experiments, the measured velocity would have an uncertainty of 0.5 mm/s. In this study of recirculation flows in a microfluidic backstep feature, velocity is in the order of tens of centimeters per second; for example, the average velocity for the lowest flow rate of 300 μL/ min used here is $\sim$5 cm/s (considering the cross section after the expansion), leading to an error in velocity measurement on the order of 1%.

The hydrodynamic size of a tracer particle is a measure of its ability to follow the flow and is found by evaluation of inertial and drag forces. According to [1], although the seeding particles need to be small in the absolute sense, for visualization of flow in a microchannel, this is not a critical concern because of the large surface-to-volume ratio at the reduced scales. The response time of a particle subjected to a step change in local fluid velocity can be used as a measure of how well the particle is able to obey the flow. For the first-order response to a constant flow acceleration (assuming Stokes flow for the particle drag), the response time is given by $\tau = d^2\rho_p/18\mu$, where d and ρ_p are the diameter and density of seeding particles, and μ is the dynamic viscosity of the fluid. For the current experiments that involve polystyrene particles in water (d: 1 μm, ρ_p: 1.05 g/cm^3), the response time of seeding particles is on the order of 1.1×10^{-6} s. The typical time interval used in the current experiment for PIV imaging is on the order of a few hundred microseconds. Comparing the response time of particles with the time interval, the particles appear to follow the flow well.

The appropriate size of particles is a compromise between Brownian motion uncertainty and the ability to faithfully follow the fluid flow, which gives the lower and upper bounds of the seeding particle diameter, respectively [15]. The average displacement of particles in the time interval of a PIV image pair of 200 μs and a velocity of 5 cm/s is 10 μm. The random displacement x_b due to Brownian motion is estimated to be 0.1 μm. This random error further reduces proportional to $\sqrt{N}$ [14] ($N = 50$ is the number of PIV image pairs used in the ensemble correlation) and becomes insignificant.

The microfluidic channels were fabricated in house. Considering the process steps, such as spin coating, photolithography pattern transfer, and PDMS casting and bonding, the imperfections in the fabrication procedure cause some variations. SU-8 spin-coating thickness determines the final height of the channels, since PDMS is cast on the SU-8 patterned mold. The spin-coating speed and the viscosity of the SU-8 PR determine the thickness of the coating. The nominal height is 100 μm; however, scanning electron microscope images showed up to a 10 μm fluctuation of height. The channel width can also vary from top to bottom of the channel due to the diffraction of exposure UV illumination in the process of photolithography. This can lead to a trapezoidal cross section instead of a rectangular section with perfect vertical walls. $\Delta w = 1.5\sqrt{\lambda \cdot z/2} \sim 6.7$ μm [11], where λ is the UV exposure wavelength, and the spin-coated PR thickness $z = 100$ μm. For a hydraulic diameter, $D_h = 4A/P = 133$ μm, the fabrication and process related error is estimated to be 8% in hydraulic diameter.

IV. Results

In this section, we investigate the effect of variation of the focus plane depth by adjusting the microscope focus and the time intervals between PIV image pairs on the flow visualization. The results at transition to recirculation flow for a backward-facing step for a 1:5 expansion are provided.

The recirculation pattern is a common feature in a backward-facing step macrochannel [8,9]. In microfluidic devices, however, the circulation zone is absent in the typical Re range of 0.01–10. In Figs. 3 and 4, laminar flow without any disturbances ($Re = 28$) and a fully developed recirculation ($Re = 280$) are shown, respectively. The Reynolds number is calculated based on a hydraulic diameter using physical properties of water. Note that, for visualizing each portion of the flow, depending on the magnitude of velocity,

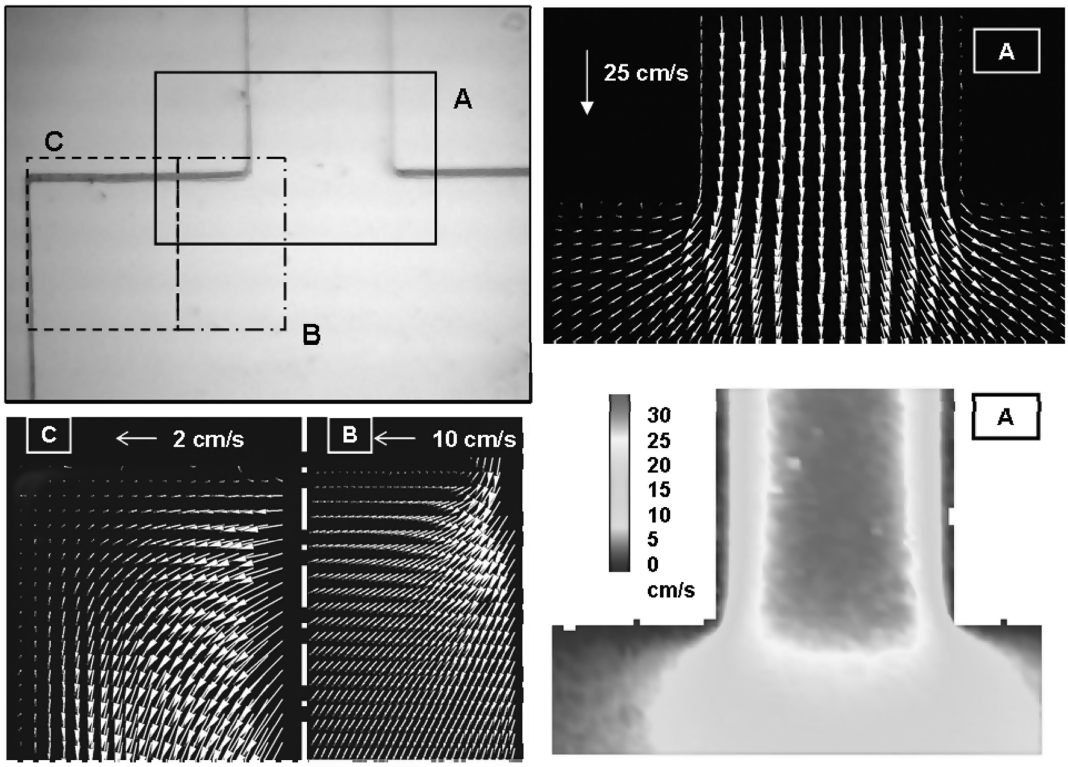

Fig. 3 Laminar flow at the backward-facing step. Because of velocity differences in different sections, sections A, B, and C were recorded using appropriate time-interval (Δt) values. ($Re = 28$).

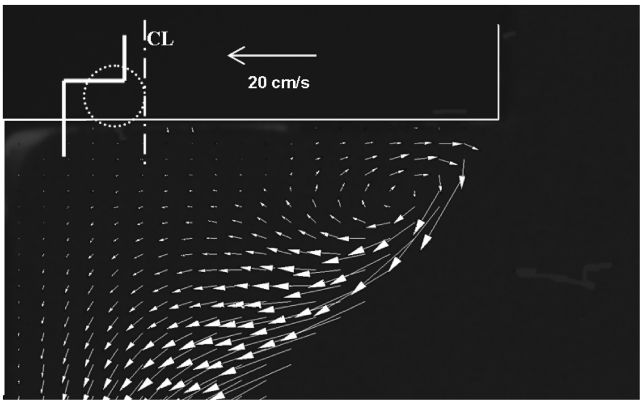

Fig. 4 Developed recirculation at the backstep ($Re = 220$).

appropriate time intervals should be used. For example, in Fig. 3, the fast-moving core is recorded using a 75 μs time interval in section A, whereas for the slow moving flow away from the center and at the corners, time intervals of 200 and 600 μs were used in visualizing sections B and C, respectively. The first signs of recirculation occur at a flow rate of $Re = 95$ (950 μL/ min).

All experiments were carried out using identical tracer particle concentrations using the same particle size of 1 μm. The weight of the individual particle is approximately 5.75×10^{-14} N. Several minutes after the flow was stopped, the particles remained dispersed and did not sediment at the bottom of the channel. Nor was there any deposition of particles centrifuged out of the recirculation zone into the corners. The average speed in the recirculation zone in the current channel was in the range of tens of centimeters per second. For an average velocity of 20 cm/s in the recirculation zone of radius 250 μm, the centrifugal force is $\sim 1.5 \times 10^{-14}$ N, which is an order of magnitude higher than the force due to gravity; however, it is still small enough to cause errors in velocity measurements.

A. Recirculation

Holding the focusing plane, the time interval, and other parameters constant, the flow rate was increased in increments of 100 μL/ min. In Fig. 5, the evolution of the recirculation is shown as the flow rate is increased. At $Re \sim 100$, the first signs of recirculation were observed at the backstep wall in the centerplane. An expansion ratio of 1:5 is potentially favorable for recirculation. The recirculation first begins at the backstep wall where it further develops and gets larger. The streamlines show that as the flow rate is increased, a larger portion of the flow is affected by the recirculation zone. The streamline that divides the circulating and noncirculating portions of the flow initially terminates on the backstep wall ($Re = 166$). The location where this dividing streamline meets the wall is called the

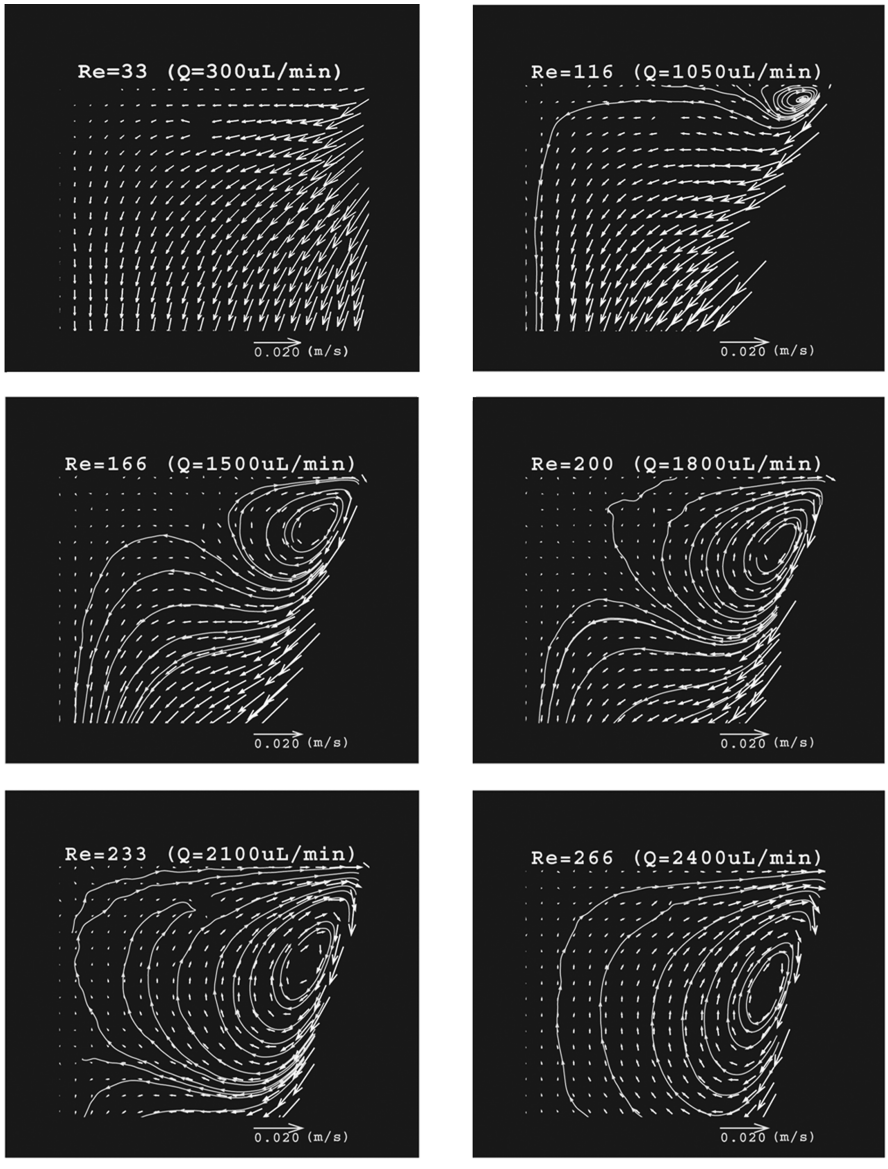

Fig. 5 Initiation and development of a recirculation zone for different *Re*.

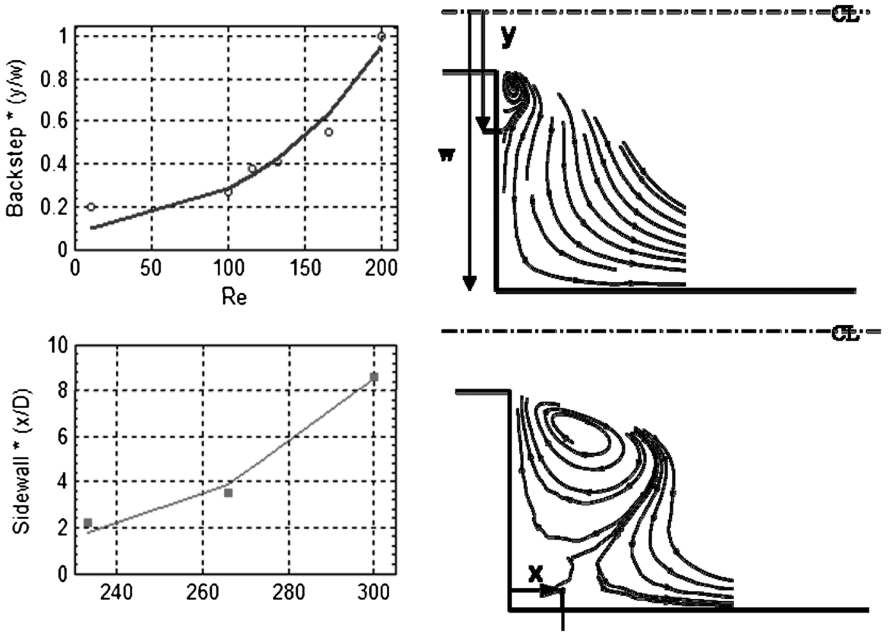

Fig. 6 Evolution of the recirculation zone. The dividing streamline migrates from the backstep wall onto the sidewalls and further downstream as flow rate increases.

reattachment point. The location of the reattachment point migrates toward the sidewalls over the backstep and then moves downstream of the channel as the flow rate is further increased (Fig. 6).

B. Volume Illumination in μPIV

If the optical parameters are kept constant, then particle visibility can be increased by either decreasing the depth of the microfluidic device or using a lower particle concentration. However, using lower particle concentration will have the effect of reducing the number of particles within each interrogation volume, resulting in noisier velocity estimates. In addition, the reduced concentration of fluorescent dye can possibly necessitate using larger interrogation spots, resulting in lower spatial resolution.

In μPIV, all the particles in the flowfield are illuminated (volume illumination) due to limited optical access. In most cases, information regarding the depthwise behavior of the flow is lost, and a 2-D average field is derived [1]. In this section, two types of depth resolution will be analyzed and compared. One is the traditional method of moving the focus plane of the microscope, which has some limitations. This is discussed in IV.B.1, which shows the limitation of this method by using two types of magnification of the microscope.

The second method of depth resolution that is discussed in IV.B.2 is to maintain the focus plane constant at the center and change the time intervals between image pairs. This method uses variable time intervals between image pairs. It is fairly well established in the literature that the cross-correlation algorithm is sensitive to the time interval between image pairs. We use this idea to bring up a functional dependency, albeit qualitatively, between Δt and depth, so that the variation of recirculation with depth can be resolved.

1. Depth Resolution Using Microscope Movement

The microscope settings were adjusted to traverse the depth of the microchannel from top to bottom. Each sidewall of the channel when observed from the top through the microscope consists of a line with two edges, because the sidewalls are not exactly vertical and the cross section slightly deviates from a rectangular to a trapezoidal shape. The edges represent the intersection of the sidewall with the top and the bottom wall. By adjusting the objective lens to be focused on the upper or lower bounds of the channel, one of the two edges would appear sharp and the other blurry. In this way, it was possible to pinpoint the upper and lower walls and calibrate the markings on the microscope focusing knobs with the actual microchannel depth. A Nikon microscope was used with two pieces of objective lenses: a 4x magnification lens (numerical aperture 0.1) that provided a depth of field of 55 μm, which is comparable to the depth of flow, and a 20x lens (numerical aperture of 0.4) that had a 5 μm depth of field. The depth cannot be resolved using a 4x magnification lens in μPIV to obtain the three-dimensional recirculation pattern at the backstep, as shown in Fig. 7. A series of PIV realizations taken at $\Delta t = 100$ μs at various focus plane depths (z^*), from the top to the bottom, shows almost the same flow pattern. In other words, the eye of the vortex, the region to which recirculation extends, and the magnitude of the velocity vectors were averaged as a 2-D field. This suggests that the ensemble cross-correlation algorithm is insensitive to the variation of the focus plane location across the channel width using lower magnification (4x objective lens). By choosing the depth of field to be significantly narrower than the depth of flow, such that only a narrow slice of the flow is in focus, the light from the seeding particles above or below the plane would be excluded as noise and do not contribute to the correlation. The depth of field can be narrowed by increasing the magnification. However, when the 20x objective was used, the area of imaging reduced significantly to the extent that only a small spot of the flow in the x-y plane could be imaged and not the overall flow, including the vortex. Using the 20x objective, the parabolic velocity profile in the depth of a straight channel could be resolved (Fig. 8) by shifting the focus plane. However, the 20x objective was not practical for the backward-facing step. Hence, one has to make a compromise between low magnification that gives a wider image area but poor depth resolution and high magnification that gives good depth resolution but narrow image area (almost a spot size). In the next section, we propose using the low magnification, which gives the wide area and variable ΔT for depth resolution.

2. Depth Resolution Using Variable Δt Between Particle-Image-Velocity Image Pairs

Time interval is an important parameter to characterize μPIV data, and its value is usually dictated by the cross-correlation algorithm settings; however, in this study, it is also used as an indirect means of resolving the depth coordinate. Various measures have been taken as shown in the literature to exclude out-of-focus particles by means of filtering functions based on light intensity [2–4]. If the light intensity is below a certain threshold for some particles, these particles would be excluded from the correlation procedure. In this work, the time interval is changed while focusing on the same plane, depending on the maximum and minimum velocity expected in the channel.

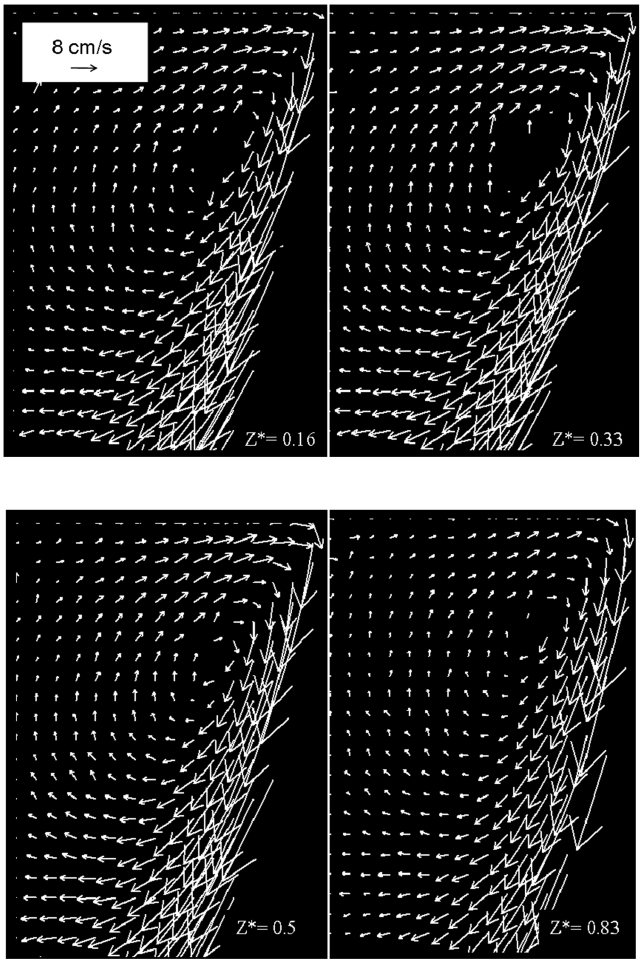

Fig. 7 μPIV realizations of a recirculation flow at different focus plane depths ($Z^* = z/H$, $\Delta t = 100$ μs, $Re = 222$). Variation of the focusing plane across the channel depth has little effect on the flow pattern for 4x magnification.

Therefore, the ensemble correlation is locked in a specific plane that contains velocities that are resolvable by the correlation scheme. Other faster- or slower-moving planes (function of depth) are excluded automatically. By tuning the time interval appropriately, the depth coordinate can be resolved. To investigate the effect of time intervals (Δt) between μPIV recordings of image pairs, the focusing plane depth, flow rate, and other parameters were kept constant.

It is seen that the correlation algorithm gets locked into a plane of flow that can be resolved within the range of parameters chosen, resulting in the most frequently occurring displacement peaks over the averaged image pairs ($z^* = 0.5$). The flowfields resulting from

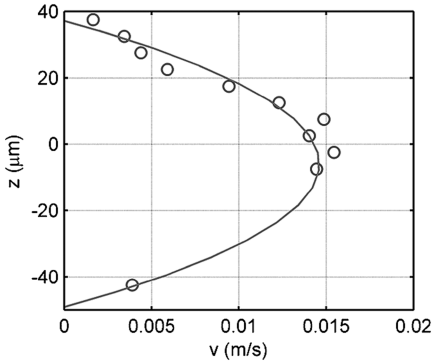

Fig. 8 Using 20x magnification (depth of field of 5 μm), the velocity across the depth of the channel can be resolved by moving the focal plane ($\Delta t = 100$ μs).

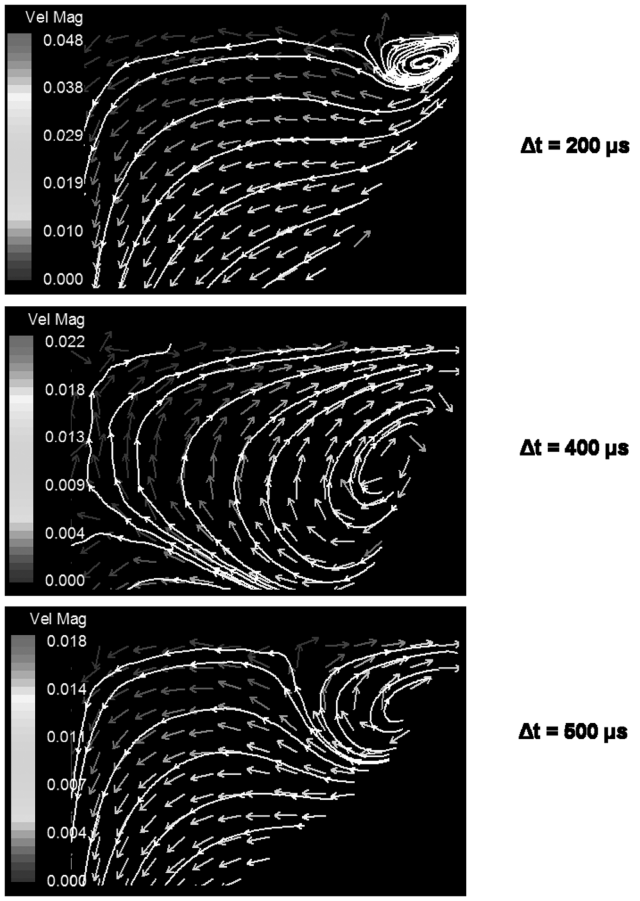

Fig. 9 μPIV realizations using different time intervals (Δt) between PIV image pairs. Focusing plane depth ($Z^* = 0.5$) and flow rate ($Re = 222$) are held constant. Resulting flow patterns differ qualitatively and quantitatively.

the three cases are significantly different for the different Δt applied in the same plane (Fig. 9). Layers of fluid moving closer to the top and bottom walls have lower velocity magnitudes compared with those close to the center of the channel. Larger time intervals are required to resolve slow-moving layers, while for the faster-moving layers at the core of the flow, shorter time intervals should be used. In this manner (for flow with a large gradient across the depth), by changing the time interval, the depth coordinate can be resolved in an indirect manner.

V. Conclusions

The backward-facing step flow was visualized in a 1:5 expansion ratio in a microchannel using the μPIV technique. The device was fabricated using the well-established SU-8 lithography and PDMS soft lithography fabrication process. Three variables were investigated while making flow visualizations. First, the flow rate was increased in increments to find out the onset of vortex generation and emergence of flow recirculation zones. The behavior of the vortex in a given plane of flow was investigated, and migration of the dividing streamline was observed; the dividing streamline initially resides on the backstep wall, gradually shifts onto the sidewall, and moves downstream as the flow rate is further increased. The flow does not get separated from the wall in normal flow rates used in microfluidic devices, even with geometrically favorable features for recirculation and separation to occur. The onset of recirculation was observed at relatively large flow rates. Second, it was observed that the cross-correlation algorithm used in this study was not sensitive to the variation of the in-focus plane location across the depth for low magnification. Finally, the algorithm was affected by the time intervals used for recording PIV double-image pairs. With a given time interval, only that portion of the flow that yields the most repeated displacement peaks in the interrogation spots is resolved as

the final output. By considering a set of μPIV realizations using incremental time intervals and combining them together, an indirect method of resolving the depth coordinate using ensemble cross-correlation schemes can be designed.

Acknowledgment

This work was partially supported by National Science Foundation Engineering Education and Centers, 0649076.

References

[1] Nguyen, N.-T., and Wereley, S. T., *Fundamentals and Applications of Microfluidics*, Artech House, London, 2002.

[2] Cummings, E. B., "An Image Processing and Optimal Nonlinear Filtering Technique for Particle Image Velocimetry of Microflows," *Experiments in Fluids*, Vol. 29, No. 7, 2000, pp. S042–S050. doi:10.1007/s003480070006

[3] Meinhart, C. D., Wereley, S. T., and Gray, M. H. B., "Volume Illumination for Two-Dimensional Particle Image Velocimetry," *Measurement Science and Technology*, Vol. 11, No. 6, 2000, p. 809. doi:10.1088/0957-0233/11/6/326

[4] Olsen, M. G., and Adrian, R. J., "Out-Of-Focus Effects on Particle Image Visibility and Correlation in Microscopic Particle Image Velocimetry," *Experiments in Fluids*, Vol. 29, No. 7, 2000, pp. S166–S174. doi:10.1007/s003480070018

[5] Olsen, M. G., and Adrian, R. J., "Brownian Motion and Correlation in Particle Image Velocimetry," *Optics and Laser Technology*, Vol. 32, No. 7–8, 2000, pp. 621–627. doi:10.1016/S0030-3992(00)00119-5

[6] Meinhart, C. D., Wereley, S. T., and Santiago, J. G., "A PIV Algorithm for Estimating Time-Averaged Velocity Fields," *Journal of Fluids Engineering*, Vol. 122, No. 2, 2000, pp. 285–289. doi:10.1115/1.483256

[7] Bourdon, C. J., Olsen, M. G., and Gorby, A. D., "Power-Filter Technique for Modifying Depth of Correlation in MicroPIV Experiments," *Experiments in Fluids*, Vol. 37, No. 2, 2004, pp. 263–271. doi:10.1007/s00348-004-0812-4

[8] Armaly, B. F., Durst, F., Pereira, J. C. F., and Schoenung, B., "Experimental and Theoretical Investigation of Backward-Facing Step Flow," *Journal of Fluid Mechanics*, Vol. 127, 1983, pp. 473–496. doi:10.1017/S0022112083002839

[9] Biswas, G., Breuer, M., and Durst, F., "Backward-Facing Step Flows for Various Expansion Ratios at Low and Moderate Reynolds Numbers," *Journal of Fluids Engineering*, Vol. 126, No. 3, 2004, pp. 362–374. doi:10.1115/1.1760532

[10] Jo, B. H., Van Lerberghe, L. M., Motsegood, K. M., and Beebe, D. J. A. B. D. J., "Three-Dimensional Micro-Channel Fabrication in Polydimethylsiloxane (PDMS) Elastomer," *Journal of Microelectromechanical Systems*, Vol. 9, No. 1, 2000, pp. 76–81. doi:10.1109/84.825780

[11] Gad-el-Hak, M., *The MEMS Handbook*, CRC Press, Boca Raton, FL, 2005.

[12] Scarano, F., and Riethmuller, M. L., "Iterative Multigrid Approach in Piv Image Processing with Discrete Window Offset," *Experiments in Fluids*, Vol. 26, No. 6, 1999, pp. 513–523. doi:10.1007/s003480050318

[13] Prasad, A. K., Adrian, R. J., Landreth, C. C., and Offutt, P. W., "Effect of Resolution on the Speed and Accuracy of Particle Image Velocimetry Interrogation," *Experiments in Fluids*, Vol. 13, No. 2, 1992, pp. 105–116. doi:10.1007/BF00218156

[14] Santiago, J. G., Wereley, S. T., Meinhart, C. D., Beebe, D. J., and Adrian, R. J., "A Particle Image Velocimetry System for Microfluidics," *Experiments in Fluids*, Vol. 25, No. 4, 1998, pp. 316–319. doi:10.1007/s003480050235

[15] Tay, F. E. H., *Microfluidics and BioMEMS Applications*, Kluwer Academic, Norwell, MA, 2002.